blood®
Regular Article

LYMPHOID NEOPLASIA

Active Akt signaling triggers CLL toward Richter transformation via overactivation of Notch1

Vivien Kohlhaas,[1-5,*] Stuart James Blakemore,[3,4,6,*] Mona Al-Maarri,[1-5,*] Nadine Nickel,[3,4,6] Martin Pal,[1-5] Andreas Roth,[3,4,6] Nadine Hövelmeyer,[7] Stephan C. Schäfer,[8] Gero Knittel,[3,4,6] Philipp Lohneis,[8] Milos Nikolic,[4,9] Janica L. Wiederstein,[3,9] Marek Franitza,[10] Theodoros Georgomonolis,[10,11] Nina Reinart,[3,4,6] Marco Herling,[3,4,6] Carmen Herling,[3,4,6] Elena M. Hartmann,[12] Andreas Rosenwald,[12] Wolfram Klapper,[13] Reinhard Büttner,[8] Riccardo Moia,[14] Davide Rossi,[15,16] Renzo Boldorini,[14,17] Gianluca Gaidano,[17] Lukas P. Frenzel,[3,4,6] Hans Christian Reinhardt,[3,4,6,18] Jens C. Brüning,[1-5] Michael Hallek,[3,4,6] Marcus Krüger,[3,9] Martin Peifer,[4,9] Christian P. Pallasch,[3,4,6,†] and F. Thomas Wunderlich[1-5,†]

[1]Max Planck Institute for Metabolism Research, Cologne, Germany; [2]Institute for Genetics, University of Cologne, Cologne, Germany; [3]Cologne Excellence Cluster on Cellular Stress Responses in Aging-Associated Diseases (CECAD), Cologne, Germany; [4]Center for Molecular Medicine Cologne (CMMC), Cologne, Germany; [5]Center for Endocrinology, Diabetes and Preventive Medicine (CEDP) Cologne, Cologne, Germany; [6]Department I of Internal Medicine, University Hospital Cologne, University of Cologne, Cologne, Germany; [7]Institute for Molecular Medicine, University Medical Center of the Johannes Gutenberg, University Mainz, Mainz, Germany; [8]Institute of Pathology, [9]Department of Translational Genomics, and [10]Cologne Center for Genomics (CCG), University of Cologne, Cologne, Germany; [11]West German Genome Center (WGGC), Cologne, Germany; [12]Institute of Pathology, University of Würzburg, and Comprehensive Cancer Center Mainfranken, Würzburg, Germany; [13]Department of Pathology, University Hospital of Schleswig-Holstein, Kiel, Germany; [14]Division of Pathology, Department of Health Science, University of Piemonte Orientale (UPO), Novara, Italy; [15]Division of Hematology, Oncology Institute of Southern Switzerland, Bellinzona, Switzerland; [16]Laboratory of Experimental Hematology, Institute of Oncology Research, Bellinzona, Switzerland; [17]Università del Piemonte Orientale, Department of Translational Medicine, Novara, Italy; and [18]Clinic for Hematology and Stem Cell Transplant, University Hospital of Essen, Essen, Germany

KEY POINTS

- **Constitutively active AKT is present in high-risk CLL and RT, and active Akt transforms murine CLL toward aggressive lymphoma.**
- **Akt orchestrates development of RT via induction of Notch1 signaling in B cells, fueled by Dll1-expressing T cells.**

Richter's transformation (RT) is an aggressive lymphoma that occurs upon progression from chronic lymphocytic leukemia (CLL). Transformation has been associated with genetic aberrations in the CLL phase involving *TP53, CDKN2A, MYC,* and *NOTCH1*; however, a significant proportion of RT cases lack CLL phase–associated events. Here, we report that high levels of AKT phosphorylation occur both in high-risk CLL patients harboring *TP53* and *NOTCH1* mutations as well as in patients with RT. Genetic overactivation of *Akt* in the murine Eμ-*TCL1* CLL mouse model resulted in CLL transformation to RT with significantly reduced survival and an aggressive lymphoma phenotype. In the absence of recurrent mutations, we identified a profile of genomic aberrations intermediate between CLL and diffuse large B-cell lymphoma. Multiomics assessment by phosphoproteomic/proteomic and single-cell transcriptomic profiles of this Akt-induced murine RT revealed an S100 protein-defined subcluster of highly aggressive lymphoma cells that developed from CLL cells, through activation of Notch via Notch ligand expressed by T cells. Constitutively active Notch1 similarly induced RT of murine CLL. We identify Akt activation as an initiator of CLL transformation toward aggressive lymphoma by inducing Notch signaling between RT cells and microenvironmental T cells. (*Blood.* 2021;137(5):646-660)

Introduction

During the clinical course of chronic lymphocytic leukemia (CLL), ~2% to 10% of patients develop an aggressive lymphoma, termed Richter's Transformation (RT).[1] RT typically displays histomorphologic characteristics similar to those of diffuse large B-cell lymphoma (DLBCL), with limited treatment options.[2-4] Transformation to RT has been shown to associate with somatic genetic events acquired in the CLL phase, including *TP53*, *CDKN2*, *MYC*, *EGR2*, or *NOTCH1*, while observed to be genetically distinct from de novo DLBCL, notably lacking recurrent mutations in genes such as *CD79B* and *BCL2*.[5,6] However, a significant proportion of cases cannot be attributed to CLL phase–associated somatic genetic events, indicating that they are required but not sufficient for driving the histologic shift.[7,8] Previous CLL phase–associated treatment, germline genetics, and aspects of CLL phase biology have also been observed to be RT risk factors, whereas the role of the tumor microenvironment (TME) in the transformation from CLL to RT has not been studied. Moreover, it has yet to be elucidated whether a central mechanism connecting these risk factors exists.

A key determinant in the pathogenesis of CLL is B-cell receptor (BCR) signaling, which mediates disease heterogeneity via either proliferation or anergy.[9,10] In the CLL phase, BCR-associated

events correlated with transformation to RT include unmutated *IGHV* (IGHV-U) status and BCR stereotypy,[11] as well as the expression of CD49d, CD38, and ZAP70. The BCR induces tonic phosphoinositol-3-kinase (PI3K)/AKT signaling believed to contribute to malignant transformation.[12,13] PI3K phosphorylates the secondary messenger PIP_2 to PIP_3 that activates the membranal kinase PDK-1 to phosphorylate PIP_3-bound AKT at the activating residue Thr308.[14,15] Downstream effects of AKT include protein synthesis, cell survival, proliferation, and glucose metabolism.[15] We therefore hypothesized that AKT activation might be the missing link in the transformation of CLL to RT.

The current study found that: (1) AKT is activated in high-risk CLL and in >50% of patients with RT; (2) constitutively active Akt promotes CLL transformation toward RT in Eμ-*TCL1* mice in vivo; (3) Notch1 is activated via constitutive Pi3k/Akt in RT cells; and (4) RT-intrinsic Notch signaling is induced by Dll1-expressing $Cd4^+$ T cells from the TME.

Materials and methods

Mouse strains and patient material

Experiments were performed according to human (medical faculty of the University of Cologne [reference no. 13-091]) and murine (LANUV 84-02.04.2014.A146 and 84-02.04.2019.A009) ethical approvals. Eμ-*TCL1* mice and *Cd19-Cre* mice were described previously and were on the C57/BL6 background.[16] To generate the *R26-fl-Akt-C* strain, a SERCA targeting vector containing a myristoylation TAG *Akt-C* was introduced into the ROSA26 locus, as previously described.[17] Finally, Eμ-*TCL1* mice were intercrossed with *Cd19-Cre*$^{Akt\text{-}C}$ mice. Furthermore, we examined *Cd19-Cre*^{FoxO1ADA} mice,[18] *Cd19-Cre*$^{Notch1\text{-}IC}$ mice,[19] and *Gsk3β* $^{S9A/wt}$ mice.[20]

Cell preparation, immunophenotyping, and multiomics profiling

Murine samples were isolated from total splenocytes, with total splenocytes used for immunophenotyping and single-cell RNA sequencing (scRNA-Seq; 10X Genomics), $Cd19^+$ MACS sorting conducted for whole-exome sequencing (WES), and phosphoproteomic/proteomic analysis. Immunophenotyping was conducted by using a standard panel by flow cytometry. WES and scRNA-Seq experiments were conducted at the Cologne Center for Genomics using standardized protocols. Phosphoproteomic/proteomic analysis was conducted as previously described.[21] Notch pathway member expression profiling was conducted via flow cytometry (MACSQuant 10 and VYB).

Immunofluorescence analysis

Murine spleens were fixed in 4% paraformaldehyde. Paraffin-embedded samples were deparaffinized and stained after retrieval. Hematoxylin and eosin staining was performed (Mayer's Hematoxylin Solution #MHS32-1L and Eosin Y Solution Aqueous #HT110232-1L; Sigma-Aldrich) according to standard protocol and imaged with AxioVision 4.2 (Carl Zeiss MicroImaging). Human sections were deparaffinized and stained with primary antibody anti-pAKT Ser473 (#3787; Cell Signaling). The sections were counterstained with 4′6-diamidino-2-phenylindole.

Immunoblot analysis

Immunoblots of murine and human samples were performed by using standard techniques with the following antibodies: anti-pAKT Ser473 (#4060 and #9271; Cell Signaling), anti-pAKT Thr308 (#4056; Cell Signaling), anti-panAKT (#4685 and #2920; Cell Signaling), pAKT (#4075; Cell Signaling), anti-pGSK3b (#9315; Cell Signaling), anti-calnexin (#208880; EMD Millipore), and anti-actin (#MAB1501; Millipore).

Further details on sample preparation, murine intercrossing, experimental conditions, and bioinformatics analysis are provided in the supplemental Methods (available on the *Blood* Web site).

Results

Active AKT is increased in high-risk CLL and RT

AKT activation in CLL cells isolated from blood of patients is heterogeneous (supplemental Figure 1A-B). To investigate whether AKT activation was associated with high-risk CLL, we screened 46 CLL patient samples with complementary targeted re-sequencing on CLL driver genes for Ser473-phosphorylation of AKT by immunoblot (Figure 1A-B). *NOTCH1*mut and *TP53*mut CLL samples had significantly increased AKT activation compared with wild type, whereas no such increase was observed in *SF3B1*mut and *ATM*mut cases. Because both *NOTCH1* and *TP53* have been associated with transformation to RT, we hypothesized that increased AKT activity could be a common mechanism of transformation. To test this theory, we immunohistochemically investigated tumor biopsy specimens from CLL (n = 8), RT (n = 19), and DLBCL (n = 12) for Ser473-phosphorylation of AKT (Figure 1C; supplemental Figure 1C). Here, increased frequency and intensity of AKT activation in RT samples were observed compared with CLL and DLBCL (CLL = 12.5%, DLBCL = 16.7%, RT = 52.6%). Furthermore, we identified that almost 50% of positively stained RT cases with complete genetic characterization carried mutations in *TP53* and *NOTCH1*. These data therefore show that active AKT is often observed in RT, both with and without somatic genetic events gained in the CLL phase.

Constitutive activation of Akt via B-cell–specific *Akt-C* expression in Eμ-*TCL1* mice reduces life span, despite similar CLL progression

To investigate whether Akt activity is sufficient to transform CLL to RT, we generated a *Rosa26* mouse model in which a loxP-flanked stop cassette precedes an N-terminal myristoylation tagged *Akt-C* version (supplemental Figure 2A-B). Upon *Cd19-Cre*–mediated recombination of the loxP-flanked stop cassette, *Akt-C* expression leads to constitutive B-cell–specific Akt-C activity due to its membranal localization in which Pdk1 activates Akt. We intercrossed Eμ-*TCL1*$^{tg/wt}$ (Eμ-*TCL1*) mice with *Cd19-Cre*$^{tg/wt}$; *R26-fl-Akt-C* (*Cd19-Cre*$^{Akt\text{-}C}$) to obtain Eμ-*TCL1*$^{tg/wt}$; *Cd19-Cre*$^{tg/wt}$ and *R26-fl-Akt-C* mice (Eμ-*TCL1*$^{Akt\text{-}C}$) (Figure 2A). Akt-C expression induced a significant increase in pAKT activity in Eμ-*TCL1*$^{Akt\text{-}C}$ vs Eμ-*TCL1* mice (supplemental Figure 2C), regardless of the fact that TCL1 is a known interaction partner and promoter of Akt in this mouse model. We followed the disease progression of Eμ-*TCL1*$^{Akt\text{-}C}$ mice in the peripheral blood, observing no significant differences in the number of $Cd19^+/Cd5^+$ cells compared with Eμ-*TCL1* mice (Figure 2B; supplemental Figure 2D). However, at ~7 months of age, Eμ-*TCL1*$^{Akt\text{-}C}$ mice quickly developed symptoms reaching euthanization criteria, whereas >80% of Eμ-*TCL1* mice remained alive at this time point (median overall survival Eμ-*TCL1*$^{Akt\text{-}C}$ vs Eμ-*TCL1*, 7.6 vs 11.6 months; $P < .001$) (Figure 2C). These data suggest

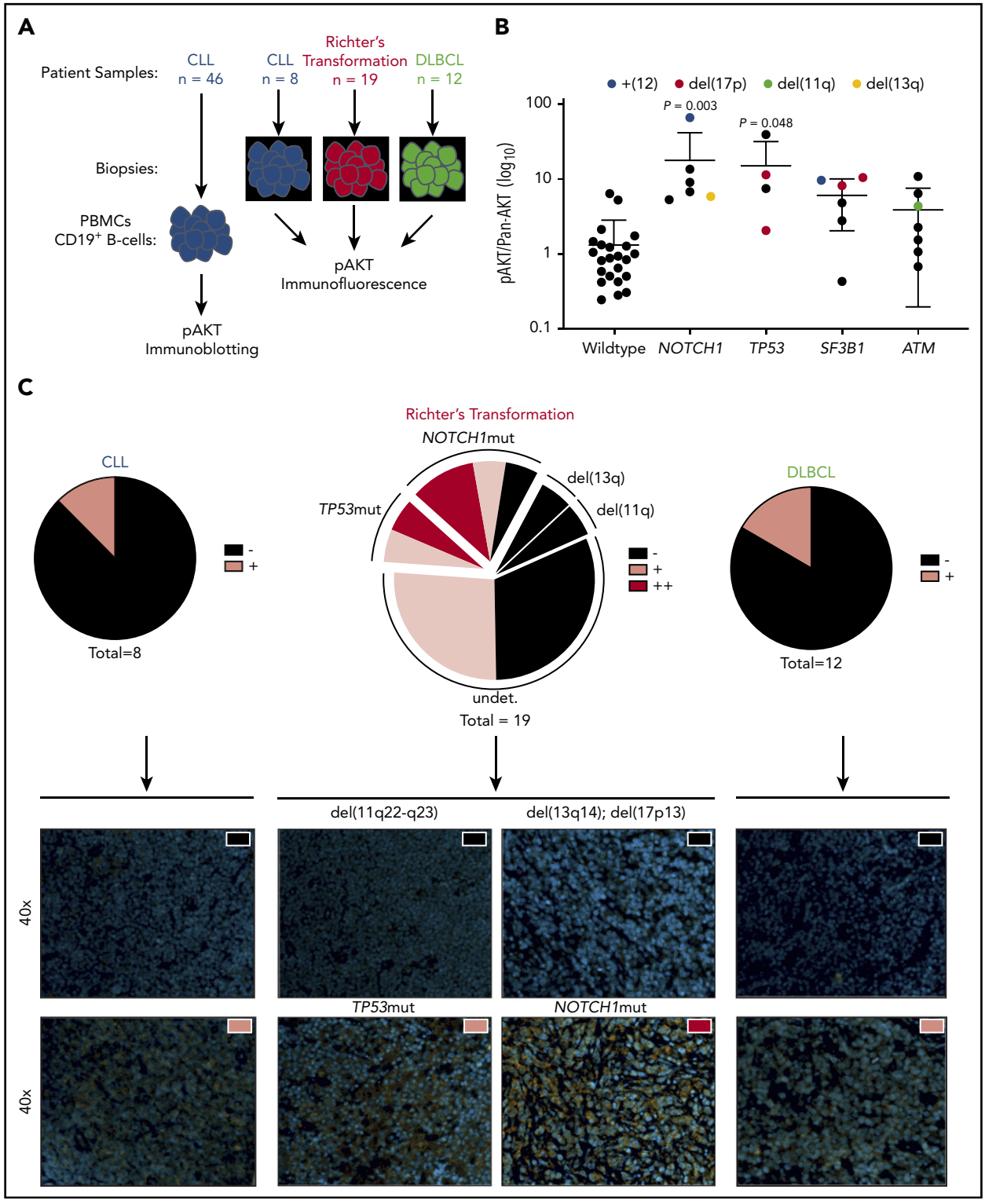

Figure 1. Increased AKT activation in CLL subsets associated with RT and increased frequency in patients with RT. (A) Flow diagram of AKT activation screening setup. (B) Histogram showing pAKT (Ser473)/panAKT expression (AKT activation) from freshly isolated peripheral B cells, in a cohort of patients with CLL stratified according to mutations in *NOTCH1, TP53, SF3B1,* and *ATM* (n = 46). Colored dots represent chromosomal aberrations identified via fluorescence in situ hybridization (blue = trisomy12; red = 17p deletion; green = 11q deletion; yellow = 13q deletion). (C) Immunofluorescence imaging of CLL (n = 8), RT (n = 19), and DLBCL (n = 12) for pAKT (Ser473). Proportion of cases defined as negative (black), positive (pink), or double positive (red) shown as pie charts for each entity (upper panel). Representative images from positive and negative cases from each entity (lower panel). All images shown at ×40 magnification. Nuclear staining (4′6-diamidino-2-phenylindole) and pAKT (Ser473) staining shown in orange. Significant differences in AKT activation between wild-type and *TP53/NOTCH1/SF3B1/ATM* mutated CLL peripheral blood mononuclear cells (PBMCs) by immunoblotting assessed by using one-way analysis of variance, with Tukey multiple comparison correction.

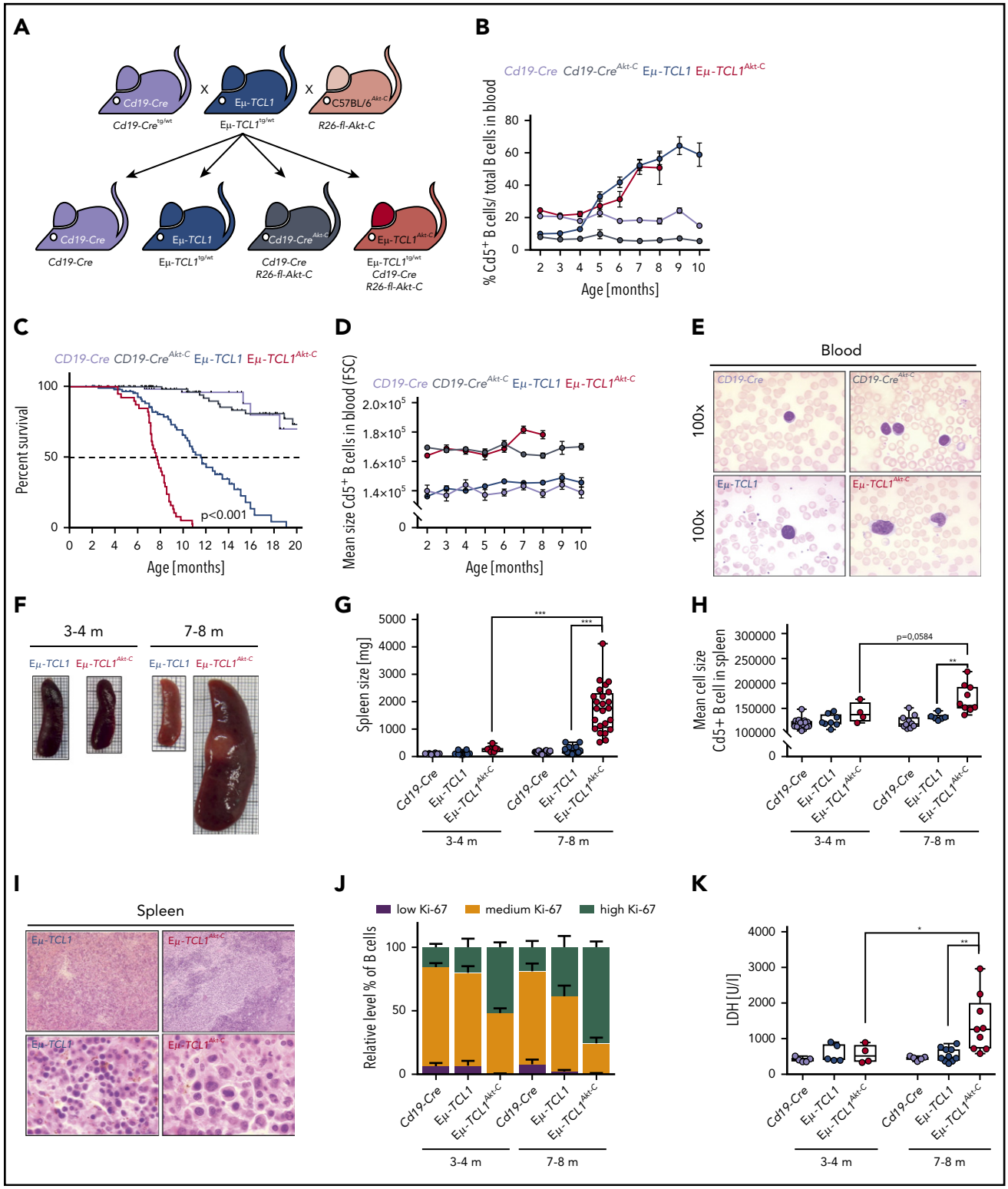

Figure 2. B-cell–specific constitutive activation of Akt in the Eμ-*TCL1* mouse model induces aggressive lymphoma with a diffuse large B-cell phenotype in vivo. (A) Breeding scheme required to generate requisite genotypes. (B) Relative quantification of Cd5$^+$ B cells from serial blood samples from *Cd19-Cre* (black), *Cd19-Cre*$^{Akt\text{-}C}$ (gray), Eμ-*TCL1* (blue), and Eμ-*TCL1*$^{Akt\text{-}C}$ (red) mice. Blood samples were measured between 2 months and 10 months of age with 1-month intervals. (C) Pairwise Kaplan-Meier overall survival analysis. Significance between groups was tested by using the pairwise log-rank *P* values. (D) Mean cell size (FSC value) of Cd5$^+$ B cells from peripheral blood measured between 2 and 10 months of age with 1-month intervals. (E) Representative hematoxylin and eosin staining of blood samples. (F) Representative images of spleens from *Cd19-Cre* (black; top left), *Cd19-Cre*$^{Akt\text{-}C}$ (gray; bottom left), Eμ-*TCL1* (blue; top right), and Eμ-*TCL1*$^{Akt\text{-}C}$ (red; bottom right) mice aged 3 to 4 months and 7 to 8 months, respectively. (G) Box plot of spleen weight for mice aged 3 to 4 months and 7 to 8 months. (H) Box plot showing the mean cell size (FSC value) within the spleen for mice aged 3 to 4 months and 7 to 8 months. (I) Representative hematoxylin and eosin staining of spleen preparations. (J) Bar graph displaying relative levels of B cells showing low, medium, and high amounts of Ki-67 in mice aged 3 to 4 months and 7 to 8 months. (K) Box plot showing the lactate dehydrogenase (LDH) levels for mice aged 3 to 4 months and 7 to 8 months. $^*P < .05$, $^{**}P \leq .01$, $^{***}P \leq .001$ (unpaired, 2-sided Student *t* test).

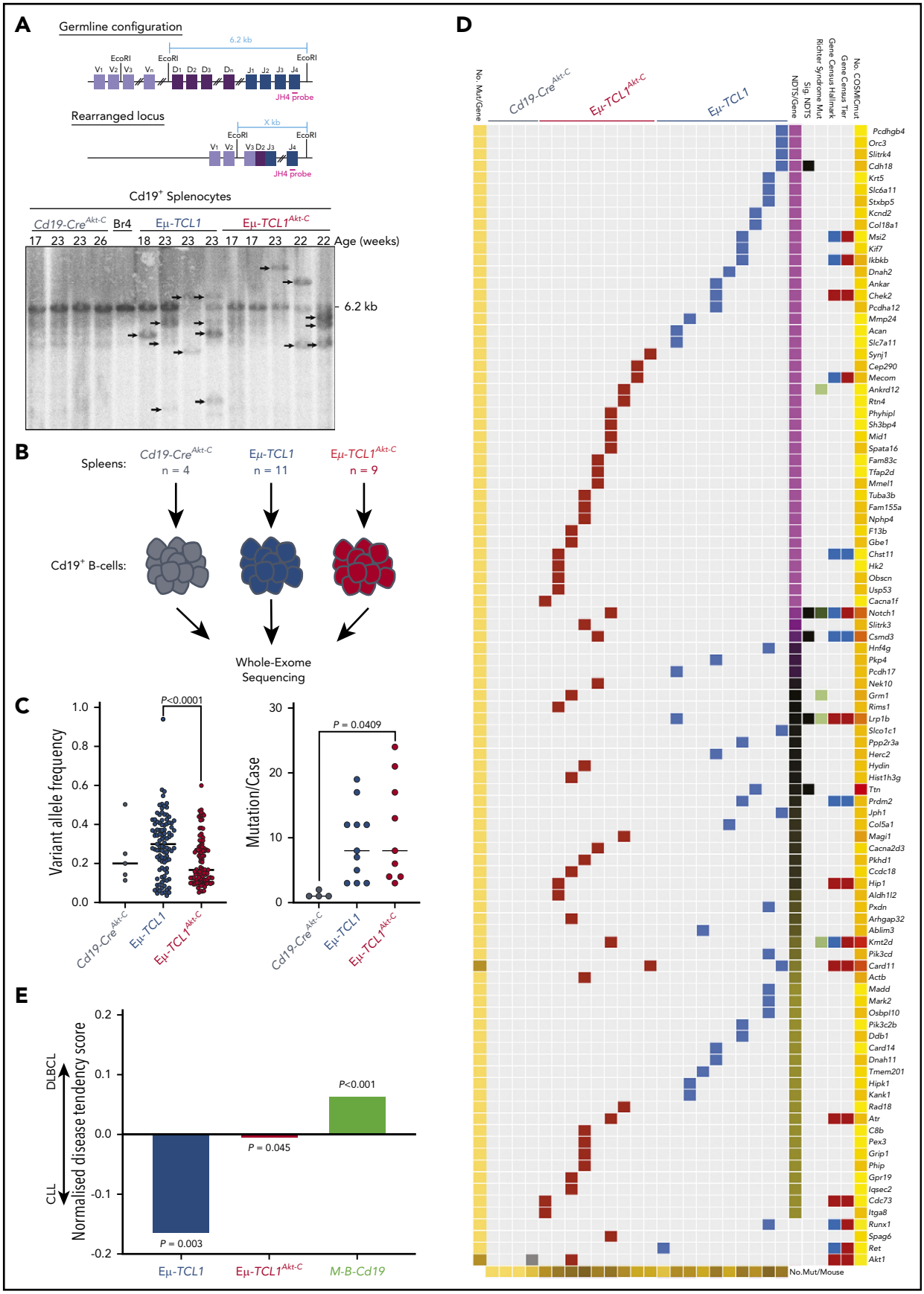

Figure 3. Catalogue Of Somatic Mutations In Cancer (COSMIC)-annotated Eμ-*TCL1*$^{Akt\text{-}C}$–mutated genes define the model as a genetically intermediary form between CLL and DLBCL. (A) Schematic strategy to identify clonal VDJ rearrangements. Using the JH4 probe on *Eco*RI-digested genomic DNA results in a 6.2 kb germline configuration band in Southern blot analysis. Clonal VDJ rearrangements indicative of B-cell leukemia and lymphoma can be identified by clear bands other than 6.2 kb (upper panel). Southern

that Akt-C leads to a dramatic reduction in overall survival, mimicking the clinical picture observed in patients with RT.

Akt-C in Eμ-*TCL1* mice drives RT

To evaluate whether Eμ-*TCL1*$^{Akt\text{-}C}$ mice had undergone transformation from CLL to RT, we examined the morphology of the malignant B cells in the peripheral blood in monthly intervals, as well as in tumor sections of spleens from mice at an age at which 100% of mice were still at risk in the Kaplan-Meier survival analysis (3-4 months) or at the median survival time of the Eμ-*TCL1*$^{Akt\text{-}C}$ mouse model (7-8 months). Although the relative cell size (FSC; forward scatter) of Cd5^{+} blood-derived B cells was enlarged in Eμ-*TCL1*$^{Akt\text{-}C}$ mice compared with Eμ-*TCL1* mice at all time points, an additional increase in relative cell size was observed at months 7 and 8 (Figure 2D). Cytomorphologic evaluation of blood smears of Eμ-*TCL1*$^{Akt\text{-}C}$ mice revealed pleomorphic blastoid cells with large degranulated nuclei and increased cytoplasm, whereas blood-derived cells in Eμ-*TCL1* mice showed round and condensed nucleoplasm (Figure 2E). Strikingly, Eμ-*TCL1*$^{Akt\text{-}C}$ mice exhibited splenomegaly at 7 to 8 months of age, accompanied by the appearance of large Cd19^{+}/Cd5^{+} blastoid cells as well as higher lactate dehydrogenase levels and reduced thrombocyte counts (Figure 2F-H,K; supplemental Figure 2E). In Eμ-*TCL1*$^{Akt\text{-}C}$ mice, hematoxylin and eosin staining revealed large blastoid cells with pleomorphic nuclei and prominent nucleoli predominating while containing frequent mitotic figures and high Ki-67 positivity (Figure 2I-J; supplemental Table 1). Importantly, these results were replicated when using *Cγ1-Cre*$^{tg/wt}$ mice as an alternative B-cell–specific *Cre*-allele to express *Akt*-C in Eμ-*TCL1* cells, recapitulating the RT phenotype with all features observed in Eμ-*TCL1*$^{Akt\text{-}C}$ mice (supplemental Figure 3A-F). Taken together, our data unequivocally show that constitutively active Akt in Eμ-*TCL1*$^{Akt\text{-}C}$ mice transforms CLL toward an aggressive DLBCL-type lymphoma defined as RT with clinical features concordant with observations in human patients.

Eμ-*TCL1*$^{Akt\text{-}C}$ mutational landscape represents an intermediary state between CLL and DLBCL

To ascertain whether Akt-C drives changes at the genomic level, we analyzed *IgH* gene rearrangements by Southern blot, revealing similar oligo-clonal characteristics in Eμ-*TCL1*$^{Akt\text{-}C}$ compared with Eμ-*TCL1* mice (Figure 3A). To investigate the impact of Akt-C, we analyzed B cells from spleens of 23 mice (Eμ-*TCL1*$^{Akt\text{-}C}$, n = 9 [aged 8-9 months]); Eμ-*TCL1*, n = 10 [aged 10-12 months], *Cd19-Cre*$^{Akt\text{-}C}$, n = 4) by WES (Figure 3B). Eμ-*TCL1*$^{Akt\text{-}C}$ were composed of mutations with significantly reduced variant allele frequency compared with Eμ-*TCL1* mice ($P < .0001$) while sharing a similar mutation burden (Figure 3C). In concordance with previous WES studies on the Eμ-*TCL1* mouse model,[22] we observed a distinct lack of recurrently mutated genes, which was also the case for Eμ-*TCL1*$^{Akt\text{-}C}$ mice (Figure 3D; supplemental Table 3.1). To elucidate the potential functional relevance of these individual gene mutations, we assessed the tendency of these genes to be mutated in human CLL and DLBCL using the cancer browser of the Catalogue Of Somatic Mutations In Cancer.[23] As an internal control, mutation data were included from a recently described murine ABC-DLBCL model (*Cd19-Cre*$^{-}$driven combined *Myd88* and *Bcl2* aberrations [*Cd19-Cre*$^{tg/wt}$;*Rosa26*$^{LSL.BCL2.IRES.GFP/wt}$;*Myd88*$^{c\text{-}p.L252P/wt}$], hereafter *M-B-Cd19*).[24] Eμ-*TCL1*–mutated genes were significantly enriched for genes mutated in CLL ($P = .003$), whereas the *M-B-Cd19* model was significantly enriched for genes mutated in DLBCL ($P < .001$). Strikingly, gene mutations in Eμ-*TCL1*$^{Akt\text{-}C}$ mice exhibited an intermediary profile between CLL and DLBCL (Figure 3E). Collectively, despite the absence of recurrent mutations, we observed an altered mutational profile in Eμ-*TCL1*$^{Akt\text{-}C}$ mice intermediary between CLL and DLBCL.

Phosphoproteomic/proteomic profiling identifies overexpression of S100a4, increased phosphorylation of Hes1, and increased activation of kinases associated with Notch signaling in Eμ-*TCL1*$^{Akt\text{-}C}$ mice

To assess the impact of active Akt on protein amount and phosphorylation, splenic B-cell–derived proteins of Eμ-*TCL1*$^{Akt\text{-}C}$ and Eμ-*TCL1* mice were investigated by using proteomics and phosphoproteomics (Figure 4A). The total amount of captured proteins remained unchanged between both genotypes, whereas Eμ-*TCL1*$^{Akt\text{-}C}$ mice showed a significant increase in the abundance of phosphorylated peptides (Figure 4B; supplemental Tables 4.1 and 4.2). The calcium-binding protein S100a4, which has previously been observed to be associated with metastatic cancer progression, was the most significantly upregulated protein in the proteomics dataset.[25] Interestingly, we observed downregulation of Nfatc1, a negative transcriptional regulator of S100a4 expression, with significantly increased phosphorylation in Eμ-*TCL1*$^{Akt\text{-}C}$ mice.[26-28] In line with this evidence, *Nfatc1* deficiency in Eμ-*TCL1* mice culminated in an aggressive lymphoma comparable to RT. In the current study, a specific role for downstream Lyn/Syk/Akt/Erk was observed to prevent nuclear Nfatc1 leading to RT.[29,30] Consistently, we observed that Lyn was significantly phosphorylated (Figure 4C) and had a marginally increased upstream kinase score in Eμ-*TCL1*$^{Akt\text{-}C}$ mice (Figure 4D; supplemental Table 4.3), suggesting that constitutively active Akt signaling may affect Nfatc1 transcriptional activity. In addition, we observed increased phosphorylation of Hes1, a prominent Notch1 target gene.[31] To reduce the dataset to the kinome level, an upstream kinase analysis was conducted by using the PhosphoSitePlus database and a simplified equation inspired by Beekhof et al (supplemental Methods).[32] This analysis identified increased activation of Wee1, Cdk4, and Csnk2b, kinases that have previously been shown to be associated with Notch signaling (Figure 4D-E).[33,34]

Figure 3 (continued) blot analysis of Cd19^{+} MACS-purified B cells derived from indicated mice using the aforementioned strategy. (B) Flow diagram of WES experimental setup. (C) Distribution of variant allele frequencies (left panel) and mutations per case (right panel) between *Cd19-Cre*$^{Akt\text{-}C}$ (n = 4), Eμ-*TCL1* (n = 10), and Eμ-*TCL1*$^{Akt\text{-}C}$ (n = 9) mice. (D) Waterfall plot of COSMIC-annotated mutations from *Cd19-Cre*$^{Akt\text{-}C}$ (n = 4), Eμ-*TCL1* (n = 10), and Eμ-*TCL1*$^{Akt\text{-}C}$ (n = 9) mice. Mutations clustered according to normalized disease tendency scores of COSMIC CLL and DLBCL mutation data (pink = CLL-associated; yellow = DLBCL-associated; black = equal distribution). Mutations were annotated for occurrence in COSMIC Cancer Gene Census Tiers (blue = animal 1; red = animal 2), COSMIC Cancer Gene Census Hallmark classification (blue = across all cancers; red = leukemia/lymphoma-specific), observed to be mutated in RT. (E) Bar graph representing the mean normalized disease tendency scores per genotype (blue = Eμ-*TCL1*; red = Eμ-*TCL1*$^{Akt\text{-}C}$; green = *M-B-Cd19*). *P* values were generated via binomial testing, presuming equal chances of each gene being mutated in either CLL or DLBCL (0.5).

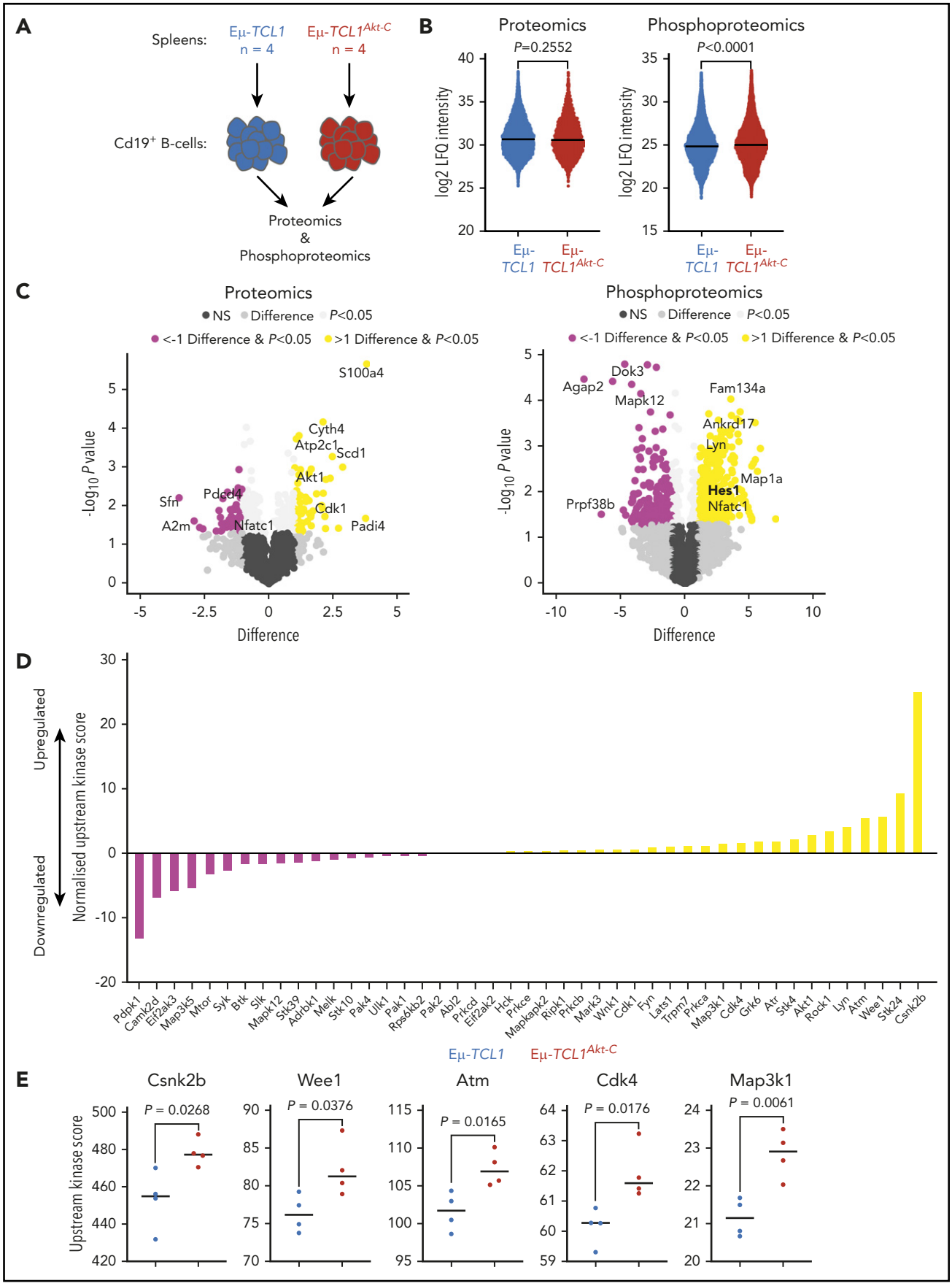
A
Spleens:
Eμ-TCL1
n = 4
Eμ-TCL1Akt-C
n = 4
Cd19+ B-cells:
Proteomics
&
Phosphoproteomics
B
Proteomics
P=0.2552
Phosphoproteomics
P<0.0001
log2 LFQ intensity
Eμ-TCL1
Eμ-TCL1Akt-C
C
Proteomics
NS
Difference
P<0.05
<-1 Difference & P<0.05
>1 Difference & P<0.05
-Log10 P value
Difference
S100a4
Cyth4
Atp2c1
Scd1
Akt1
Sfn
Pdcd4
Cdk1
A2m
Nfatc1
Padi4
Phosphoproteomics
Agap2
Dok3
Mapk12
Fam134a
Ankrd17
Lyn
Map1a
Hes1
Nfatc1
Prpf38b
D
Upregulated
Downregulated
Normalised upstream kinase score
Pdpk1
Camk2d
Eif2ak3
Map3k5
Mtor
Syk
Btk
Slk
Mapk12
Stk39
Adrbk1
Melk
Stk10
Pak4
Ulk1
Pak1
Rps6kb2
Pak2
Abl2
Prkcd
Eif2ak2
Hck
Prkce
Mapkapk2
Ripk1
Prkcb
Mark3
Wnk1
Cdk1
Fyn
Lats1
Trpm7
Prkca
Map3k1
Cdk4
Grk6
Atr
Stk4
Akt1
Rock1
Lyn
Atm
Wee1
Stk24
Csnk2b
Eμ-TCL1
Eμ-TCL1Akt-C
E
Csnk2b
Wee1
Atm
Cdk4
Map3k1
Upstream kinase score
P = 0.0268
P = 0.0376
P = 0.0165
P = 0.0176
P = 0.0061

Figure 4.

Notably, a reciprocal regulation between Notch and Nfatc1 has been reported in numerous cancer types.[35,36]

scRNA-Seq identifies an aggressive B-cell subpopulation in Eμ-*TCL1*$^{Akt\text{-}C}$ defined by cell–cell interactions and overactivation of Notch

To analyze the transcriptomic profiles of the aggressive subclones arising from indolent CLL in the Eμ-*TCL1*$^{Akt\text{-}C}$ mice, we characterized splenocytes via scRNA-Seq (Figure 5A). After implementing per-sample preprocessing and clustering using standard settings, we integrated all samples, leading to a dataset of 33 224 cells composed of 21 clusters (Figure 5B; supplemental Figure 5.1; supplemental Table 5.1). Genotype-specific cell number increases were observed within clusters, notably in the malignant B cells, in which 5 clusters were observed to be enriched or shared between Eμ-*TCL1*$^{Akt\text{-}C}$ and Eμ-*TCL1* (clusters encircled in red), whereas 2 clusters were observed to be enriched in Eμ-*TCL1* mice (clusters encircled in blue). To unravel the transcriptional differences between Eμ-*TCL1*$^{Akt\text{-}C}$ and Eμ-*TCL1* cells within the enriched/shared clusters (RT-C1 to RT-C5), we conducted differential expression (DE) analysis across all cells, identifying 570 significantly DE genes supplemental Table 5.2). We then tested for gene ontology (GO) enrichment using all 570 significant genes, from which we calculated the disease tendency of each GO term to be composed of genes significantly upregulated in either Eμ-*TCL1*$^{Akt\text{-}C}$ or Eμ-*TCL1* mice (supplemental Table 5.3). This analysis identified an enrichment of cell–cell interaction-associated GO terms composed of Eμ-*TCL1*$^{Akt\text{-}C}$ significant genes, with TCR/BCR signaling also being increased in Eμ-*TCL1*$^{Akt\text{-}C}$ mice. We delved deeper into the cell–cell interaction GO terms via network visualization (Figure 5C), identifying a profile of Eμ-*TCL1*$^{Akt\text{-}C}$ upregulated genes associated with S100 signaling (*S100a4, S100a9*), Notch signaling (*Hes1, Cd44, Itga4* [*Cd49d*], *Cd86, Flna, Zmiz1*), and Pi3k/Akt signaling (*Pik3r1*), as well as the immune checkpoint gene *Cd274* (*Pd-l1*) (Figure 5D). Significantly upregulated genes exhibited variable transcription factor binding sites for FoxO1, Nfatc1, and Rbpjκ (Notch1) in their 2 kb upstream promoter region, suggesting a direct transcriptional link between these transcription factors in *Akt-C*–expressing cells. Importantly, increased *S100a4* expression was validated in B cells from Eμ-*TCL1*$^{Akt\text{-}C}$ mice that were dependent on Nfatc1 and Rbjκ/Notch regulation but not on FoxO1 in B cells derived from *Gsk3β*$^{S9A/+}$(Nfatc1 nuclear-excluded), *Cd19-Cre*$^{tg/wt}$; *R26-fl-Notch1-IC* (*Cd19-Cre*$^{Notch\text{-}IC}$ nuclear-active Notch1), and *Cd19-Cre*$^{tg/wt}$; *R26-fl-FoxO1ADA* (*Cd19-Cre*^{FoxO1ADA} nuclear FoxO1) (supplemental Figure 5.2A-B). Furthermore, we validated increased expression for *Hes1* at the RNA level and for Pd-l1 at the protein level in B cells from Eμ-*TCL1*$^{Akt\text{-}C}$ mice. In conclusion, we identified a specific aggressively transformed cluster in the Eμ-*TCL1*$^{Akt\text{-}C}$ mice appearing among the indolent leukemic B cells defined by Akt-mediated cell–cell interaction associated transcriptional regulation as well as a Notch/S100-protein signature corresponding to the aggressive nature of RT.

scRNA-Seq identifies that prosurvival signaling drives enrichment of *Cd4*$^{+}$ T cells in the TME of Eμ-*TCL1*$^{Akt\text{-}C}$ mice

To further explore the potential biological importance of upregulation of the cell–cell interaction signature in the malignant B cells, we analyzed the TME in the integrated single-cell dataset, identifying an enrichment of *Cd4*$^{+}$ T cells in Eμ-*TCL1*$^{Akt\text{-}C}$ mice compared with Eμ-*TCL1* and *Cd19-Cre* mice (Figure 5E). DE gene analysis between Eμ-*TCL1*$^{Akt\text{-}C}$ and Eμ-*TCL1* cells was conducted, identifying 483 significantly DE genes; upon GO analysis, we observed a lack of GO terms with a disease tendency score indicative of Eμ-*TCL1*$^{Akt\text{-}C}$ enrichment (B cells = 24% >0.1, Cd4^{+} T cells = 0.42% >0.1) (supplemental Tables 5.4 to 5.5; supplemental Figure 5.2C). Therefore, we assessed the GO terms enriched for genes significantly upregulated in Eμ-*TCL1* cells, identifying programmed cell death–associated GO terms to be a predominant feature in Eμ-*TCL1* mice (Figure 5F). However, we observed that the distribution of proapoptotic to antiapoptotic genes differed between the two genotypes, with Eμ-*TCL1*$^{Akt\text{-}C}$ cells proportionally composed of more antiapoptotic genes (supplemental Figure 5.2D). Importantly, these genes included central players in prosurvival signaling, such as *Bcl2*, as well as other genes involved in T-cell biology (*Ccr7* and *Il4*) (Figure 5G). Finally, these antiapoptotic Eμ-*TCL1*$^{Akt\text{-}C}$ upregulated genes were often found in the GO terms that were indicative of Eμ-*TCL1*$^{Akt\text{-}C}$ enrichment, further supporting their importance in the milieu of upregulated genes in the *Cd4*$^{+}$ T cells of the Eμ-*TCL1*$^{Akt\text{-}C}$ TME. In summary, we identified a TME population that may have been elicited to proliferate with increased prosurvival capacity via the RT malignant clone.

Overactivation of Notch signaling in Eμ-*TCL1*$^{Akt\text{-}C}$ RT cells is supported by concomitant Dll1 overexpression on Cd4^{+} T cells

Our experimental data from CLL and RT patient biopsy specimens, in combination with the multiomics assessment of the Eμ-*TCL1*$^{Akt\text{-}C}$ mouse model, provide various lines of evidence that active Akt signaling drives Notch activation in CLL to RT transformation (Figure 6A). To consolidate these findings, we assessed the RNA expression of Notch receptors (*Notch1-4*) in the malignant B cells, observing significant increases in expression of *Notch1* and *Notch3* in Eμ-*TCL1*$^{Akt\text{-}C}$ vs Eμ-*TCL1* mice as well as Notch target gene regulation (Figure 6B; supplemental Figure 6A). Moreover, significantly higher protein levels of Notch1 were observed in Eμ-*TCL1*$^{Akt\text{-}C}$ mice displaying a fully transformed RT phenotype at 7 to 8 months of age but not in mice at 3 to 4 months (Figure 6C). Importantly, only the Cd5^{+} RT cells revealed Notch1 expression, whereas Cd5^{-} B cells from the same mouse exhibited levels similar to CLL cells (Figure 6D). Notch1 is activated after ligand-binding presented on adjacent cells, namely Jagged (Jag) and delta-like (Dll) proteins.[37-39] To specify the ligand-presenting cells, we analyzed protein levels of

Figure 4. Overexpression of S100a4, increased phosphorylation of Hes1, and increased activation of Cdk4 and Wee1 infer Notch1 activation. (A) Flow diagram of phosphoproteomic/proteomic experimental setup. (B) Log_2 label-free quantification (LFQ) intensity values of all proteins captured (left panel) or phosphopeptides (right panel) across all mice per genotype. (C) Volcano plots representing the difference in log_2 LFQ intensity of proteins (left panel) and phosphopeptides (right panel) between Eμ-*TCL1* (n = 4) and Eμ-*TCL1*$^{Akt\text{-}C}$ (n = 4) mice. Significant DE proteins/phosphopeptides defined as difference >1 and $P < .05$ (upregulated in Eμ-*TCL1*$^{Akt\text{-}C}$ = yellow; downregulated = pink). (D) Normalized upstream kinase scores for all 45 kinases with available PhosphoSitePlus kinome data. Bars represent the difference in upstream kinase scores between Eμ-*TCL1* (n = 4) and Eμ-*TCL1*$^{Akt\text{-}C}$ (n = 4) (upregulated in Eμ-*TCL1*$^{Akt\text{-}C}$ = yellow; downregulated = pink). (E) Upstream kinase scores from the top significantly upregulated kinases in Eμ-*TCL1*$^{Akt\text{-}C}$ mice. Significant differences between groups assessed by using Student *t* test, significant proteins/peptides defined as $P < .05$ as well as difference >1 /<1 for phosphoproteomics/proteomics, whereas for upstream kinase analysis. $P < .05$ kinases were considered significant. NS, not significant.

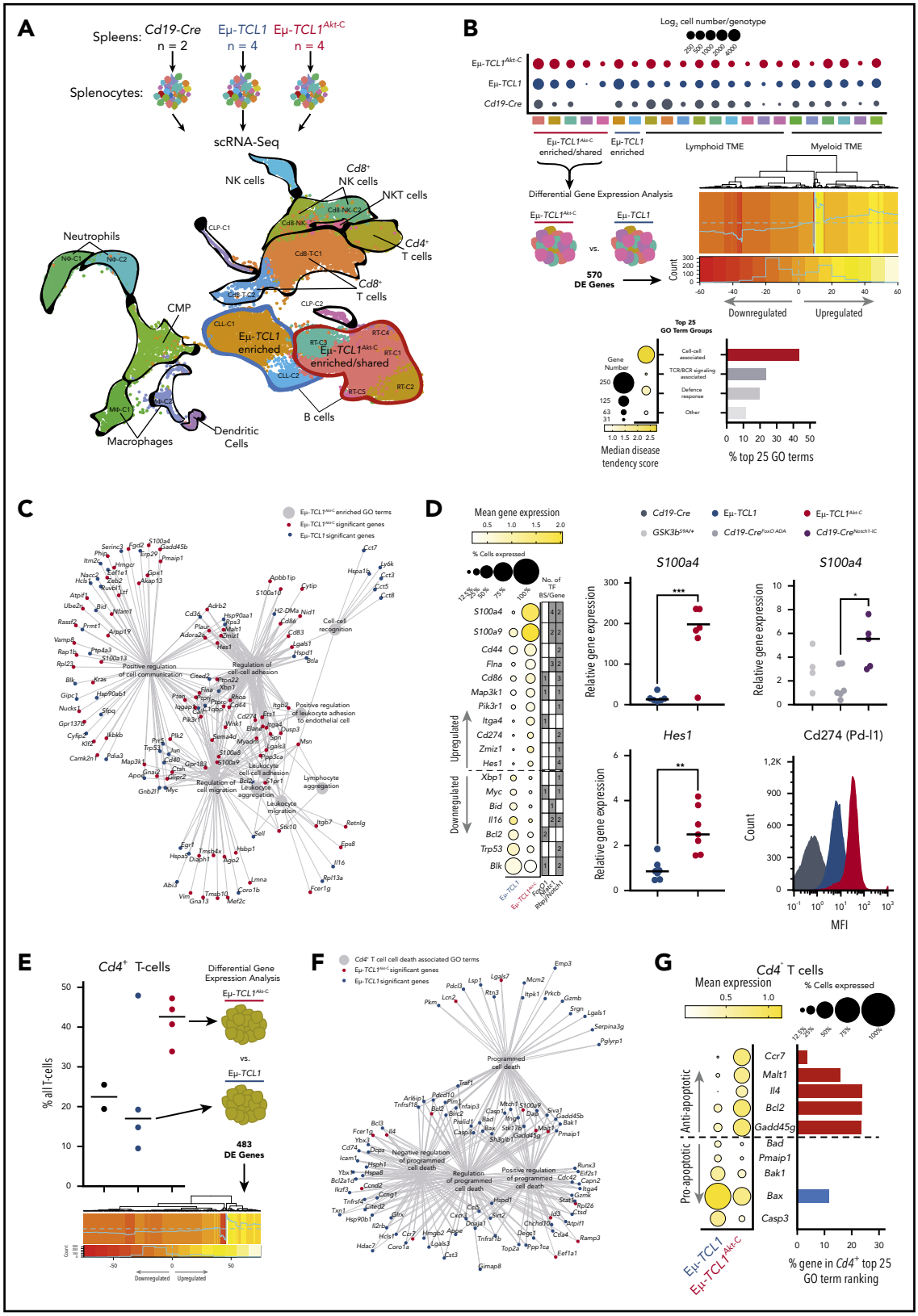

Figure 5. Cell–cell interactions and overexpression of *S100a4/Hes1/Cd274*(Pd-l1) defines RT gene signature in Eμ-*TCL1*$^{Akt\text{-}C}$–enriched B-cell clusters. (A) Flow diagram of scRNA-Seq experimental setup (upper panel). Integrated UMAP from *Cd19-Cre* (n = 2), Eμ-*TCL1* (n = 4), and Eμ-*TCL1*$^{Akt\text{-}C}$ (n = 4) mice (n = 33 224 cells). Demarked clusters represent B-cell tumor clusters enriched within either Eμ-*TCL1* (blue) or Eμ-*TCL1*$^{Akt\text{-}C}$ (red) and the TME (black). (B) Dot plot representing the number of cells appearing in each cluster per genotype (upper panel). Graphical representation of differential gene expression analysis and heatmap showing the normalized percent cell expression changes of significantly differentially expressed genes (middle panel). Dot plot representing the median disease tendency score of GO term groups with the dot size representing the number of genes associated with all GO terms (lower panel, left graph). Bar chart representing the percentage of GO term groups of the top 25 Eμ-*TCL1*$^{Akt\text{-}C}$–associated GO

Dll1 in splenic cells. Interestingly, we observed significantly increased levels of Dll1 ligand on T cells, but not on other TME cells nor on the RT cells of Eμ-*TCL1*$^{Akt\text{-}C}$ mice displaying a fully transformed RT phenotype with specific expression on Cd4$^+$ T cells (Figure 6E-H; supplemental Figure 6B-C). Because Os et al showed that Cd4$^+$ T cells support the survival and proliferation of CLL cells, we decided to assess the proportion of Cd4$^+$/Cd8$^+$ T cells in both genotypes.[40] Importantly, we observed a significantly enriched proportion of Cd4$^+$ Foxp3$^+$ T cells in Eμ-*TCL1*$^{Akt\text{-}C}$ mice, whereas the Cd8$^+$ T-cell population remained unchanged (Figure 6I-K). In summary, these data show that RT cells are supported by Dll1-expressing Cd4$^+$ T cells to induce Notch1 overactivation.

B-cell–intrinsic *Notch1-IC* expression in Eμ-*TCL1* mice recapitulates the Eμ-*TCL1*$^{Akt\text{-}C}$ RT phenotype

To elucidate whether CLL to RT transformation via Notch1 could be driven intrinsically in the Eμ-*TCL1* mouse model, we used a conditional model of constitutively activated *Notch1-IC*[19] intercrossed with Eμ-*TCL1* and *Cd19-Cre* mice (Eμ-*TCL1*$^{Notch1\text{-}IC}$) (supplemental Figure 7A). The initial disease development of Cd19$^+$/Cd5$^+$ B cells in the blood of Eμ-*TCL1*$^{Notch1\text{-}IC}$ mice was significantly slower than in Eμ-*TCL1* mice (supplemental Figure 7B). Mice did not show reduced survival compared with Eμ-*TCL1* mice, which could be explained due to altered B-cell differentiation affected by the *Notch1-IC* allele.[41] However, once Cd5$^+$ B cells appeared in the blood, these mice rapidly succumbed to the disease, with a survival trajectory comparable to that of Eμ-*TCL1*$^{Akt\text{-}C}$ mice (Figure 7A). At that age, Eμ-*TCL1*$^{Notch1\text{-}IC}$ mice presented with massive splenomegaly, which was confirmed as RT showing a disrupted splenic architecture with blastoid cells (Figure 7B-D). Furthermore, we observed that the malignant B cells of Eμ-*TCL1*$^{Notch1\text{-}IC}$ mice were significantly increased in size compared with Eμ-*TCL1* counterparts (Figure 7E), while also having significantly higher active Akt levels (Figure 7F; supplemental Figure 7C). Finally, Eμ-*TCL1*$^{Notch1\text{-}IC}$ mice did not show concomitant Dll1 overexpression on T cells in the TME, confirming that constitutive activation of Notch1 is sufficient to drive CLL to RT transformation without TME support (Figure 7G-H; supplemental Figure 7D-E**)**. In conclusion, constitutive activation of Notch1 in Eμ-*TCL1* mice recapitulates the transformed phenotype of aggressive lymphoma and functionally identifies the Akt and Notch1 signaling axis as key determinants of murine RT. Our model therefore clarifies that what occurs in CLL toward RT in mice must be further validated in human patients.

Discussion

Our analysis showed increased frequency of active AKT in primary RT samples to CLL samples, as well as in CLL samples with high-risk mutations for RT, such as those carrying *TP53* and *NOTCH1* mutations. This indicates that active AKT signaling represents a key feature in disease progression beyond the immediate contribution of respective oncogenic drivers.

To elucidate the functional impact of active Akt on CLL disease pathogenesis, we crossed the Eμ-*TCL1* mouse model with a construct driving constitutive Akt activation specifically in B cells. This method induced an aggressive lymphoma phenotype with very high disease penetrance, mimicking the clinical features of RT, namely slow disease development followed by sudden progression with DLBCL-like morphology. This phenotype was only observed in combination with Eμ-*TCL1*, which compared with a lack of cancer-associated mutations in *Cd19-Cre*$^{Akt\text{-}C}$ mice supports the notion that constitutively active Akt alone is not sufficient to drive leukemia/lymphomagenesis. Although it has been proposed that *TCL1* prolongs Akt activation,[42] the constitutive activation of Akt provided by the *Rosa26* construct used in this study was significantly higher than what can be achieved by *TCL1* overexpression alone.

Although genomic analyses of Eμ-*TCL1* and Eμ-*TCL1*$^{Akt\text{-}C}$ mice failed to identify recurrent mutated genes, a profile defined by our "disease tendency score" categorized Eμ-*TCL1*$^{Akt\text{-}C}$ mice as having an intermediary mutational signature between CLL and DLBCL. Notwithstanding the preferential occurrence of genes associated with RT in the Eμ-*TCL1*$^{Akt\text{-}C}$ model, including *Notch1* does suggest a shared mechanism between murine and human RT.

To trace these respective mechanisms, our multiomics analysis revealed increased Notch signaling and the upregulation of S100-proteins in Eμ-*TCL1*$^{Akt\text{-}C}$ cells by various means. In patients with RT, the most frequently acquired mutation is activating *NOTCH1* (30% of all mutations).[5,6,43] The evolutionary conserved Notch1 signaling affects proliferation, maturation, and survival of B cells[44-46] and is induced by cell–cell interaction in which Dll ligands on one cell type bind to Notch receptors on another to proteolytically process the Notch intracellular domain (NICD) that represents the active moiety to regulate gene expression.[37] The S100-protein family has been implicated in various malignancies as mediators of proliferation.[25] In particular, S100A4 has

Figure 5 (continued) terms (lower panel, right graph). (C) Network visualization of all cell–cell associated GO terms from the analysis conducted in B. GO terms denoted as large gray circles, Eμ-*TCL1*$^{Akt\text{-}C}$ and Eμ-*TCL1* significant genes denoted as small red and blue circles, respectively, and gray lines represent the association between genes and GO terms. (D) Dot plot of selected cell–cell associated GO term genes with biological links to Notch signaling, Pi3k/Akt signaling, or RT. Size of the dots represents the percentage of cells with a normalized expression value >1, with the color of the dots representing the mean expression of each gene across all cells within the cluster. Additional annotation beside the dot plot represents the number of transcription factor–binding sites for all 25 genes for FoxO1, Nfatc1, and Rbpjκ/Notch1, respectively (left panel). Messenger RNA expression validation in Cd19$^+$ splenocytes for *S100a4* and *Hes1* genes in Eμ-*TCL1* and Eμ-*TCL1*$^{Akt\text{-}C}$ mice, as well as *S100a4* in *Gsk3β*$^{S9A/+}$ (Nfatc1 nuclear excluded), *Cd19-Cre*$^{tg/wt}$; *R26-fl-Notch1-IC* (*Cd19-Cre*$^{Notch1\text{-}IC}$ nuclear *Notch1*), and *Cd19-Cre*$^{tg/wt}$; *R26-fl-FoxO1ADA* (*Cd19-Cre*^{FoxO1ADA} nuclear *FoxO1*) via quantitative polymerase chain reaction. Protein expression validation in CD19$^+$ splenocytes for Cd274 (Pd-l1) in *Cd19-Cre*, Eμ-*TCL1*, and Eμ-*TCL1*$^{Akt\text{-}C}$ mice (right panel). (E) Percentage of Cd4$^+$ T cells per mouse per genotype as a function of all T cells (left panel). Graphical representation of differential gene expression analysis of Cd4$^+$ T cells (right panel) and heatmap showing the normalized percent cell expression changes of significantly differentially expressed genes (lower panel panel). (F) Network visualization of all cell death–associated GO terms from the analysis conducted in E. GO terms denoted as large gray circles, Eμ-*TCL1*$^{Akt\text{-}C}$ and Eμ-*TCL1* significant genes denoted as small red and blue circles, and gray lines represent the association between genes and GO terms. (G) Dot plot of selected cell death–associated GO term genes. Size of the dots represents the percentage of cells with a normalized expression value >1, with the color of the dots representing the mean expression of each gene across all cells within the cluster (left panel). Bar chart representing in percent terms how often the genes presented occur in the top 25 Eμ-*TCL1*$^{Akt\text{-}C}$–associated GO terms, with red bars for Eμ-*TCL1*$^{Akt\text{-}C}$ significant genes and blue bars for Eμ-*TCL1* significant genes. $^*P < .05$, $^{**}P \leq .01$, $^{***}P \leq .001$ (unpaired, 2-sided Student *t* test). CLP, common lymphoid progenitor; CMP, common myeloid progenitor; MFI, mean fluorescent intensity; NK, natural killer; NKT, natural killer T.

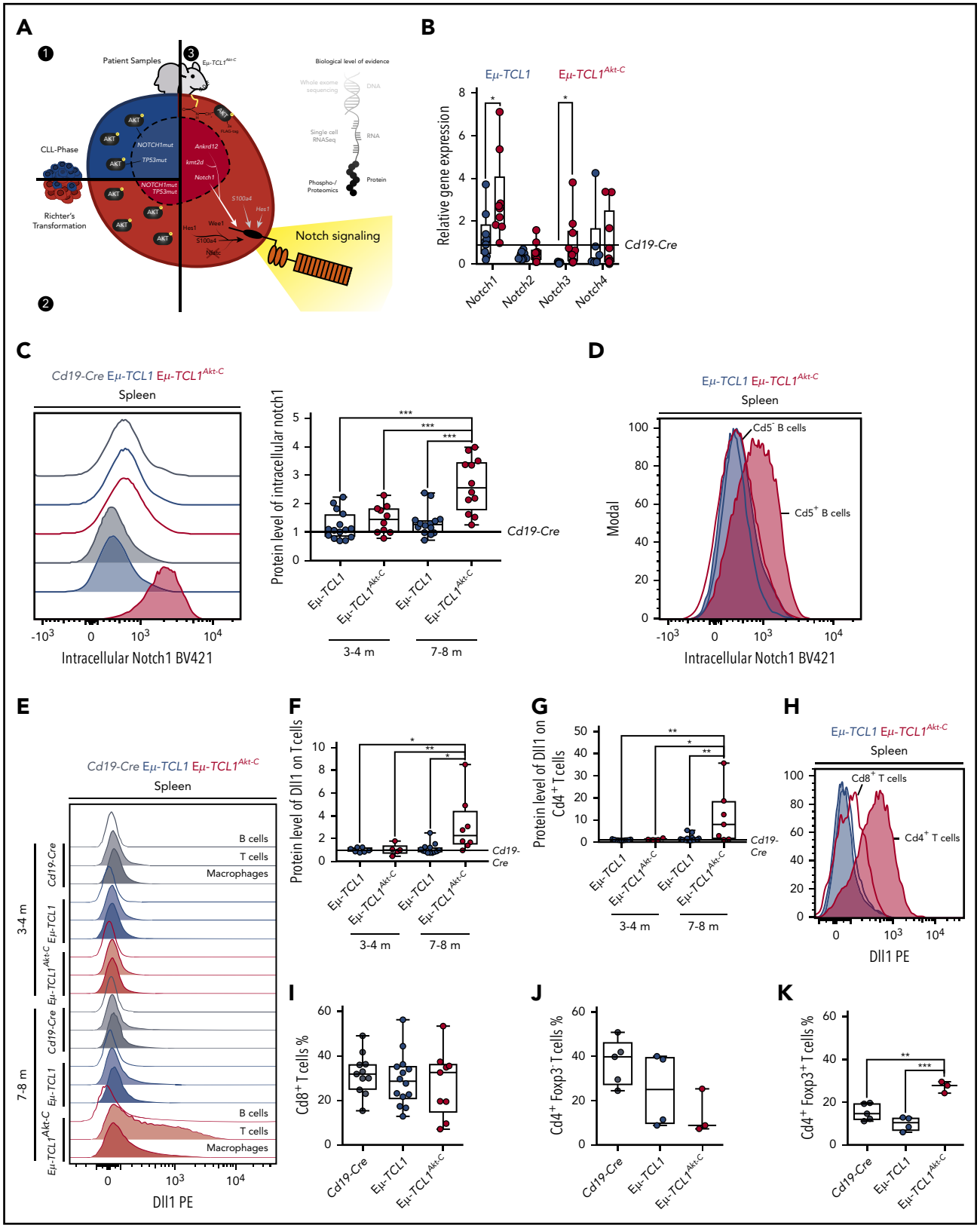

Figure 6. Notch1 activation supported via Dll1 from Cd4⁺ T cells. (A) Graphic representing the identification of Notch1 signaling as a central component of all data presented in Figures 1 to 5. (B) Messenger RNA quantification of *Notch* receptors and (C) representative blot and relative protein quantification of activated Notch1 in Eμ-*TCL1* and Eμ-*TCL1*$^{Akt\text{-}C}$ mice at 3 to 4 months and 7 to 8 months via flow cytometry, respectively. (D) Representative blot of activated Notch1 in Cd5⁻ and Cd5⁺ B cells via flow cytometry in Eμ-*TCL1* and Eμ-*TCL1*$^{Akt\text{-}C}$ mice at 7 to 8 months. (E) Representative blot and relative protein quantification of Dll1 in B cells, T cells, and macrophages in Eμ-*TCL1* and Eμ-*TCL1*$^{Akt\text{-}C}$ mice at 3 to 4 months and 7 to 8 months via flow cytometry. (F) Dll1 phycoerythrin (PE) on splenic T cells at 3 to 4 months and 7 to 8 months. (G) Dll1 PE on splenic Cd4⁺ T cells at 3 to 4 months and 7 to 8 months. (H) Representative blot of Dll1 on splenic Cd4⁺ and Cd8⁺ T cells in Eμ-*TCL1* and Eμ-*TCL1*$^{Akt\text{-}C}$ mice at 7 to 8 months. (I) Percentage of Cd8⁺ T cells from *Cd19-Cre*, Eμ-*TCL1*, and Eμ-*TCL1*$^{Akt\text{-}C}$ mice. Respective quantification of Cd4⁺ Foxp3⁻ T cells (J) and of Cd4⁺ Foxp3⁺ regulatory T cells (K). $^{*}P < .05$, $^{**}P \leq 0.01$, $^{***}P \leq .001$ (unpaired, 2-sided Student *t* test).

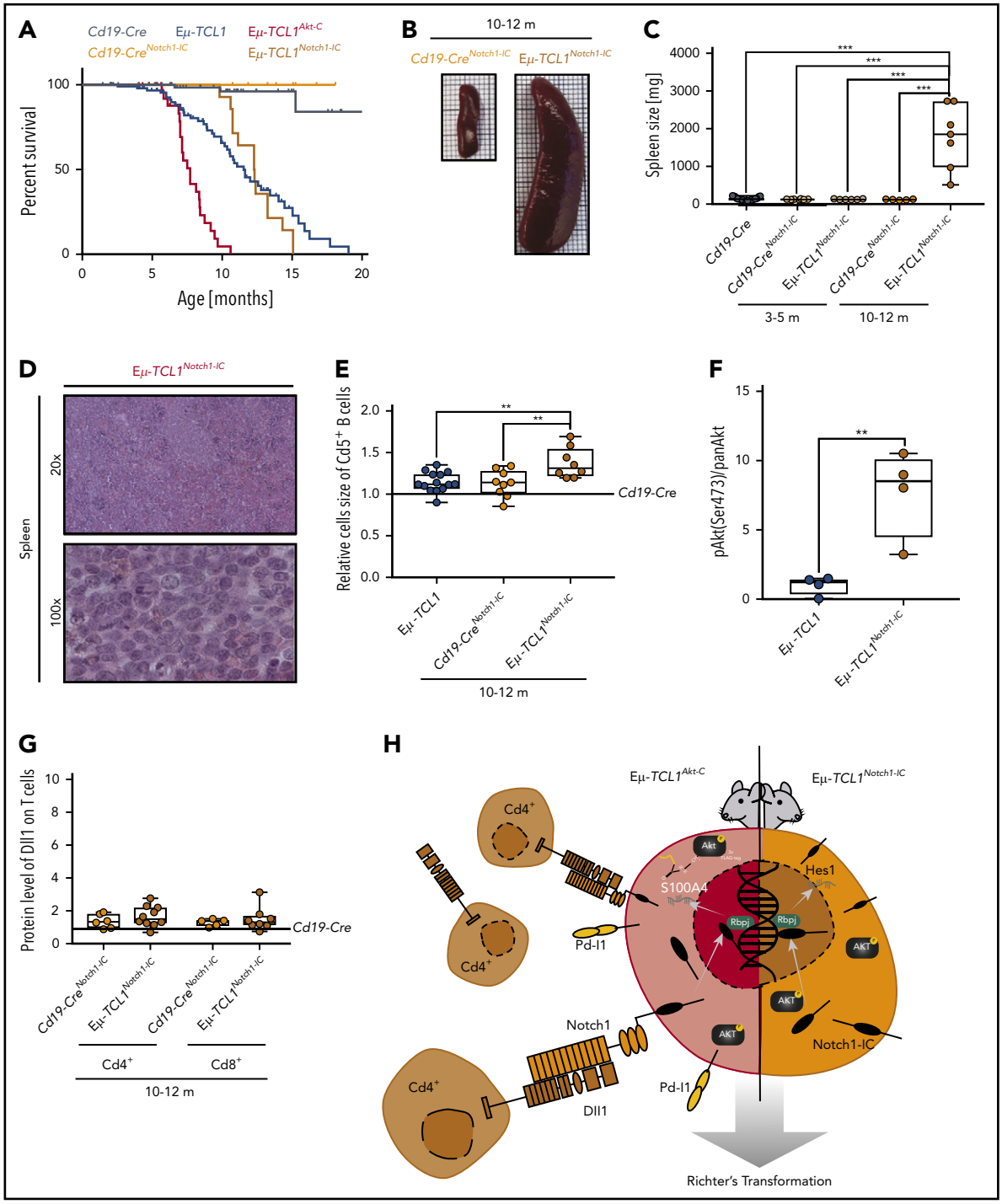

Figure 7. Constitutively active Notch-IC drives RT. (A) Pairwise Kaplan-Meier overall survival analysis for *Cd19-Cre*$^{Notch1\text{-}IC}$ (yellow) vs Eμ-*TCL1*$^{Notch1\text{-}IC}$ (orange) mice; for comparison included from Figure 2 were *Cd19-Cre* (black), *Cd19-Cre*$^{Akt\text{-}C}$ (gray), Eμ-*TCL1* (blue), and Eμ-*TCL1*$^{Akt\text{-}C}$ (red) mice. (B) Representative images of spleens from *Cd19-Cre*$^{Notch1\text{-}IC}$ vs Eμ-*TCL1*$^{Notch1\text{-}IC}$ mice aged 10 to 12 months. (C) Box plot of spleen weight for mice aged 10 to 12 months. (D) Representative hematoxylin and eosin staining of spleen preparations derived from Eμ-*TCL1*$^{Notch1\text{-}IC}$ mice showing DLBCL-like morphology. (E) Relative mean cell size (FSC) of Cd5$^+$ splenic B cells aged 10 to 12 months. (F) Box plot showing pAkt (Ser473)/panAKT quantified from immunoblot of supplemental Figure 7D. (G) Box plot showing *Dll1* protein level of Cd4$^+$ T cells from Eμ-*TCL1*$^{Notch1\text{-}IC}$ mice. (H) Graphical abstract displaying Notch1 functional role in RT. $^{**}P \leq .01$, $^{***}P \leq .001$ (unpaired, 2-sided Student *t* test).

been implicated in relapsed/refractory DLBCL[47] as well as a potential target in AML,[48] with a functional role in metastasis and cytokine release.[25]

Here, we observed in relation to Notch signaling increased *Hes1* expression and phosphorylation and increased activity of Wee1 and Cdk4 in RT cells via phosphoproteomics/proteomics. *Hes1* is a bona fide target gene of Notch signaling,[31] whereas Wee1 and Cdk4 have been previously observed to be associated with Notch signaling activation.[33,34] Furthermore, in the scRNA-Seq analysis, we identified a cell–cell interaction GO term profile in Eμ-*TCL1*$^{Akt\text{-}C}$ enriched/shared clusters, with

significantly increased expression of genes involved in S100-protein and Notch signaling, including; *S100a4, S100a9, Cd44, Itga4* (*Cd49d*), *Hes1, Flna,* and *Zmiz1*. S100A4 has been shown to be regulated by both Notch and PI3K/AKT signaling in head and neck cancers (10.1158/0008-5472.CAN-10-2350), and S100A9 has been implicated in interleukin-17–induced NOTCH1 activation of oligodendrocyte progenitor cells in demyelinating disease.[49] Cd44 and Cd49d have both been implicated as high-risk markers in CLL,[50,51] with Cd44 also shown to synergize with Notch1 to drive T-cell acute lymphoblastic leukemia in vivo,[52] whereas Cd49d has been associated with trisomy 12 status and *NOTCH1*mut status, both of which are associated with CLL to RT transformation.[53,54] Finally, such Akt-Notch1 interactions have also been previously reported in a drosophila screen and in T-cell acute lymphoblastic leukemia.[55,56] Furthermore, an Akt/Notch2-IC synergism promotes B-cell differentiation toward the marginal zone compartment.[41] Taken together, all these findings suggest the overactivation of Notch signaling driven by constitutive Akt activation and vice versa.

Clearly, Akt-mediated transcriptional control regulates Notch expression also in nontransformed cells; however, because we were only able to validate Notch1 activation and target gene upregulation in RT cells, we expanded our perspective toward the TME as a potential source of stimulating ligands. Here, we identified a specific increase of $Cd4^+$ $Foxp3^+$ T cells in the Eμ-$TCL1^{Akt\text{-}C}$ mice with increased prosurvival capacity, which we later characterized as having increased Dll1 ligand expression. We hypothesize that the constitutive activation of Akt drives a cell–cell interaction program that elicits the expansion of $Cd4^+$ T cells and overexpression of Dll1, which in turn provides Notch1 activation facilitating CLL to RT transformation. This hypothesis is supported by our data that Eμ-$TCL1^{Akt\text{-}C}$ mice have sudden disease onset between 6 and 8 months, while already showing increased Notch1 expression but lacking active Notch1-IC pretransformation. Beyond this hypothesis, we show the transformative potential of active Notch1 signaling in Eμ-$TCL1^{Notch1\text{-}IC}$ mice displaying complete histomorphologic features of aggressive RT.

Ultimately, our data suggest that aggressive transformation of indolent lymphomas does not only depend on the acquisition of genomic aberrations but may also be initiated by a changed functional status of a potentially oncogenic signaling pathway fueled from the TME. This model will allow further elucidation of targeted RT therapies, including PI3K/AKT and immune checkpoint inhibition approaches. Particularly, we are able to model immune checkpoint inhibition and target TME interactions such as NOTCH1 to combine these approaches to overcome refractory RT.[57,58] Finally, pAKT might be considered a new biomarker for high-risk CLL, and combined inhibition of PI3K/AKT and NOTCH1 might represent a potential treatment option for high-risk CLL and RT patients with active AKT.

Acknowledgments

The authors are indebted to their patients who contributed tissue and blood samples to this study. They are grateful for technical assistance from Cathy Baitzel, Reinhild Brinker, Brigitte Hampel, Patrick Jankowski, Anke Lietzau, Michael Michalik, Yvonne Meyer, Christiane Schäfer, Pia Schol, and Nadine Spenrath. The authors also thank Janine Altmueller and Peter Nuernberg at the Cologne Center for Genomics for outstanding support.

This work was supported by the German Research Foundation (DFG; KFO 286) RP5 (F.T.W. and C.P.P.), RP6 (M.H.), RP1 (M.H.), and CP2 (R.B. and C.H.). C.P.P. was supported by the Foerderprogramm Nachwuchsforschungsgruppen NRW 2015–2021, CAP Program of the Center for Molecular Medicine Cologne, and a research grant by Gilead Sciences.

Authorship

Contribution: C.P.P., S.J.B., and F.T.W. wrote the manuscript; V.K., S.J.B., M.A., M. Hallek, C.P.P., and F.T.W. designed the experiments. V.K., S.J.B., M.A., N.N., M.P., A.R., N.H., G.K., N.R., C.H., J.C.B., C.P.P., and F.T.W. performed experiments and analyzed the data; P.L., C.H., M. Herling, E.M.H., A.R., W.K., R.B., R.M., D.R., R.B., G.G., L.P.F., H.C.R., M. Hallek, S.J.B., and C.P.P. provided clinical samples and analyzed clinical data; S.J.B., M.P., and C.P.P. and performed DNA WES analysis; S.J.B., M.N., M.P., M.F., T.G., and C.P.P. performed scRNA-Seq analysis; V.K., J.L.W., M.K., and S.J.B. performed mass spectrometry analysis; H.C.R., M.P., S.C.S., N.H., N.R., M. Herling, and C.H. provided analytical tools; and all authors read, revised, and approved the manuscript.

Conflict-of-interest disclosure: The authors declare no competing financial interests.

ORCID profiles: S.J.B., 0000-0003-2892-1162; S.C.S., 0000-0002-2116-1212; T.G., 0000-0002-4066-9257; W.K., 0000-0001-7208-4117; M. Peifer, 0000-0002-5243-5503; C.P.P., 0000-0001-5675-6905; F.T.W., 0000-0002-9209-3501.

Correspondence: Christian P. Pallasch, Department I of Internal Medicine I, University Hospital of Cologne, Kerpener Str. 62, 50937 Cologne, Germany; e-mail: christian.pallasch@uk-koeln.de; or F. Thomas Wunderlich, MPI for Metabolism Research, Gleueler Str. 5050931 Cologne, Germany; e-mail: thomas.wunderlich@sf.mpg.de.

Footnotes

Submitted 9 March 2020; accepted 7 July 2020; prepublished online on *Blood* First Edition 2 November 2020. DOI 10.1182/blood.2020005734.

The mass spectrometry proteomics data have been deposited to the ProteomeXchange Consortium via the PRIDE [1] partner repository with the data set identifier PXD017457; Project Name: Active AKT Signaling triggers CLL towards Richter's transformation via over-activation of Notch1; Project accession: PXD017457; Project DOI: not applicable; Reviewer account details: username: reviewer50015@ebi.ac.uk, password: wc6QIlL8.

*V.K., S.J.B., and M.A. contributed equally to this study as first authors.

†C.P.P. and F.T.W. contributed equally to this study as senior authors.

The online version of this article contains a data supplement.

There is a *Blood* Commentary on this article in this issue.

The publication costs of this article were defrayed in part by page charge payment. Therefore, and solely to indicate this fact, this article is hereby marked "advertisement" in accordance with 18 USC section 1734.

REFERENCES

1. Richter MN. Generalized reticular cell sarcoma of lymph nodes associated with lymphatic leukemia. *Am J Pathol*. 1928;4(4):285-NaN, 7.
2. Rossi D, Gaidano G. Richter syndrome: pathogenesis and management. *Semin Oncol*. 2016;43(2):311-319.
3. Jain N, Keating MJ. Richter transformation of CLL. *Expert Rev Hematol*. 2016;9(8):793-801.
4. Parikh SA, Kay NE, Shanafelt TD. How we treat Richter syndrome. *Blood*. 2014;123(11):1647-1657.
5. Fabbri G, Khiabanian H, Holmes AB, et al. Genetic lesions associated with chronic lymphocytic leukemia transformation to Richter syndrome. *J Exp Med*. 2013;210(11):2273-2288.
6. Rossi D, Spina V, Deambrogi C, et al. The genetics of Richter syndrome reveals disease heterogeneity and predicts survival after transformation. *Blood*. 2011;117(12):3391-3401.
7. Rossi D, Cerri M, Capello D, et al. Biological and clinical risk factors of chronic lymphocytic leukaemia transformation to Richter syndrome. *Br J Haematol*. 2008;142(2):202-215.
8. Young E, Noerenberg D, Mansouri L, et al. EGR2 mutations define a new clinically aggressive subgroup of chronic lymphocytic leukemia. *Leukemia*. 2017;31(7):1547-1554.
9. Stevenson FK, Krysov S, Davies AJ, Steele AJ, Packham G. B-cell receptor signaling in chronic lymphocytic leukemia. *Blood*. 2011;118(16):4313-4320.
10. Packham G, Krysov S, Allen A, et al. The outcome of B-cell receptor signaling in chronic lymphocytic leukemia: proliferation or anergy. *Haematologica*. 2014;99(7):1138-1148.
11. Rossi D, Spina V, Cerri M, et al. Stereotyped B-cell receptor is an independent risk factor of chronic lymphocytic leukemia transformation to Richter syndrome. *Clin Cancer Res*. 2009;15(13):4415-4422.
12. Ringshausen I, Schneller F, Bogner C, et al. Constitutively activated phosphatidylinositol-3 kinase (PI-3K) is involved in the defect of apoptosis in B-CLL: association with protein kinase Cdelta. *Blood*. 2002;100(10):3741-3748.
13. Yahiaoui OI, Nunès JA, Castanier C, et al. Constitutive AKT activation in follicular lymphoma. *BMC Cancer*. 2014;14(1):565.
14. Stephens L, Anderson K, Stokoe D, et al. Protein kinase B kinases that mediate phosphatidylinositol 3,4,5-trisphosphate-dependent activation of protein kinase B. *Science*. 1998;279(5351):710-714.
15. Manning BD, Cantley LC. AKT/PKB signaling: navigating downstream. *Cell*. 2007;129(7):1261-1274.
16. Asslaber D, Qi Y, Maeding N, et al. B-cell-specific IRF4 deletion accelerates chronic lymphocytic leukemia development by enhanced tumor immune evasion. *Blood*. 2019;134(20):1717-1729.
17. Belgardt BF, Husch A, Rother E, et al. PDK1 deficiency in POMC-expressing cells reveals FOXO1-dependent and -independent pathways in control of energy homeostasis and stress response. *Cell Metab*. 2008;7(4):291-301.
18. Stöhr O, Schilbach K, Moll L, et al. Insulin receptor signaling mediates APP processing and β-amyloid accumulation without altering survival in a transgenic mouse model of Alzheimer's disease. *Age (Dordr)*. 2013;35(1):83-101.
19. Murtaugh LC, Stanger BZ, Kwan KM, Melton DA. Notch signaling controls multiple steps of pancreatic differentiation. *Proc Natl Acad Sci U S A*. 2003;100(25):14920-14925.
20. McManus EJ, Sakamoto K, Armit LJ, et al. Role that phosphorylation of GSK3 plays in insulin and Wnt signalling defined by knockin analysis. *EMBO J*. 2005;24(8):1571-1583.
21. Bansal A, Neuhaus R, Izquierdo-Alvarez E, et al ATM-mediated DNA damage response in macrophages primes phagocytosis and immune checkpoint regulation. *bioRxiv*. 2020; doi: https://doi.org/10.1101/2020.03.14.987438
22. Zaborsky N, Gassner FJ, Höpner JP, et al. Exome sequencing of the TCL1 mouse model for CLL reveals genetic heterogeneity and dynamics during disease development. *Leukemia*. 2019;33(4):957-968.
23. Tate JG, Bamford S, Jubb HC, et al. COSMIC: the Catalogue Of Somatic Mutations In Cancer. *Nucleic Acids Res*. 2019;47(D1):D941-D947.
24. Knittel G, Liedgens P, Korovkina D, et al; German International Cancer Genome Consortium Molecular Mechanisms in Malignant Lymphoma by Sequencing Project Consortium. B-cell-specific conditional expression of Myd88p.L252P leads to the development of diffuse large B-cell lymphoma in mice. *Blood*. 2016;127(22):2732-2741.
25. Ambartsumian N, Klingelhöfer J, Grigorian M. The multifaceted S100A4 protein in cancer and inflammation. *Methods Mol Biol*. 2019;1929:339-365.
26. Bhattacharyya S, Deb J, Patra AK, et al. NFATc1 affects mouse splenic B cell function by controlling the calcineurin—NFAT signaling network. *J Exp Med*. 2011;208(4):823-839.
27. Mak TW, Grusdat M, Duncan GS, et al. Glutathione primes T cell metabolism for inflammation [published correction appears in *Immunity*. 2017;46(6):1089-1090]. *Immunity*. 2017;46(4):675-689.
28. Beals CR, Sheridan CM, Turck CW, Gardner P, Crabtree GR. Nuclear export of NF-ATc enhanced by glycogen synthase kinase-3. *Science*. 1997;275(5308):1930-1934.
29. Müller DJ, Wirths S, Fuchs AR, et al. Loss of NFAT2 expression results in the acceleration of clonal evolution in chronic lymphocytic leukemia. *J Leukoc Biol*. 2019;105(3):531-538.
30. Märklin M, Heitmann JS, Fuchs AR, et al. NFAT2 is a critical regulator of the anergic phenotype in chronic lymphocytic leukaemia. *Nat Commun*. 2017;8(1):755.
31. De Obaldia ME, Bell JJ, Wang X, et al. T cell development requires constraint of the myeloid regulator C/EBP-α by the Notch target and transcriptional repressor Hes1. *Nat Immunol*. 2013;14(12):1277-1284.
32. Beekhof R, van Alphen C, Henneman AA, et al. INKA, an integrative data analysis pipeline for phosphoproteomic inference of active kinases. *Mol Syst Biol*. 2019;15(4):e8250.
33. Joshi I, Minter LM, Telfer J, et al. Notch signaling mediates G1/S cell-cycle progression in T cells via cyclin D3 and its dependent kinases. *Blood*. 2009;113(8):1689-1698.
34. Duan Y, Dong X, Nie J, et al. Wee1 kinase inhibitor MK-1775 induces apoptosis of acute lymphoblastic leukemia cells and enhances the efficacy of doxorubicin involving downregulation of Notch pathway. *Oncol Lett*. 2018;16(4):5473-5481.
35. Zanotti S, Smerdel-Ramoya A, Canalis E. Reciprocal regulation of Notch and nuclear factor of activated T-cells (NFAT) c1 transactivation in osteoblasts. *J Biol Chem*. 2011;286(6):4576-4588.
36. Zanotti S, Canalis E. Notch suppresses nuclear factor of activated T cells (NFAT) transactivation and Nfatc1 expression in chondrocytes. *Endocrinology*. 2013;154(2):762-772.
37. Bray SJ. Notch signalling in context. *Nat Rev Mol Cell Biol*. 2016;17(11):722-735.
38. Bray SJ. Notch signalling: a simple pathway becomes complex. *Nat Rev Mol Cell Biol*. 2006;7(9):678-689.
39. Okosun J, Wolfson RL, Wang J, et al. Recurrent mTORC1-activating RRAGC mutations in follicular lymphoma [published correction appears in *Nat Genet*. 2016;48(6):700]. *Nat Genet*. 2016;48(2):183-188.
40. Os A, Bürgler S, Parente Ribes A, et al. Chronic lymphocytic leukemia cells are activated and proliferate in response to specific T helper cells. *Cell Rep*. 2013;4(3):566-577.
41. Hampel F, Ehrenberg S, Hojer C, et al. CD19-independent instruction of murine marginal zone B-cell development by constitutive Notch2 signaling. *Blood*. 2011;118(24):6321-6331.
42. Pekarsky Y, Koval A, Hallas C, et al. Tcl1 enhances Akt kinase activity and mediates its nuclear translocation. *Proc Natl Acad Sci U S A*. 2000;97(7):3028-3033.
43. Fabbri G, Dalla-Favera R. The molecular pathogenesis of chronic lymphocytic leukaemia. *Nat Rev Cancer*. 2016;16(3):145-162.
44. Arruga F, Vaisitti T, Deaglio S. The NOTCH pathway and its mutations in mature B cell malignancies. *Front Oncol*. 2018;8:550.
45. He Y, Pear WS. Notch signalling in B cells. *Semin Cell Dev Biol*. 2003;14(2):135-142.
46. Kang JA, Kim WS, Park SG. Notch1 is an important mediator for enhancing of B-cell activation and antibody secretion by Notch ligand. *Immunology*. 2014;143(4):550-559.
47. Fornecker LM, Muller L, Bertrand F, et al. Multi-omics dataset to decipher the complexity of drug resistance in diffuse large B-cell lymphoma. *Sci Rep*. 2019;9(1):895.
48. Alanazi B, Munje CR, Rastogi N, et al. Integrated nuclear proteomics and transcriptomics identifies S100A4 as a therapeutic

target in acute myeloid leukemia. *Leukemia*. 2020;34(2):427-440.

49. Wang C, Zhang CJ, Martin BN, et al. IL-17 induced NOTCH1 activation in oligodendrocyte progenitor cells enhances proliferation and inflammatory gene expression. *Nat Commun*. 2017;8(1):15508.

50. Gutjahr JC, Greil R, Hartmann TN. The role of CD44 in the pathophysiology of chronic lymphocytic leukemia. *Front Immunol*. 2015; 6:177.

51. Dal Bo M, Tissino E, Benedetti D, et al. Functional and clinical significance of the integrin alpha chain CD49d expression in chronic lymphocytic leukemia. *Curr Cancer Drug Targets*. 2016;16(8):659-668.

52. García-Peydró M, Fuentes P, Mosquera M, et al. The NOTCH1/CD44 axis drives pathogenesis in a T cell acute lymphoblastic leukemia model. *J Clin Invest*. 2018;128(7): 2802-2818.

53. Zucchetto A, Caldana C, Bomben R, et al. CD49d is overexpressed in trisomy 12 chronic lymphocytic leukemia by an epigenetic-dependent transcriptional control. *Blood*. 2012;120(21):929.

54. Benedetti D, Tissino E, Pozzo F, et al. NOTCH1 mutations are associated with high CD49d expression in chronic lymphocytic leukemia: link between the NOTCH1 and the NF-κB pathways. *Leukemia*. 2018;32(3): 654-662.

55. Villegas SN, Gombos R, García-López L, et al. PI3K/Akt cooperates with oncogenic notch by inducing nitric oxide-dependent inflammation. *Cell Rep*. 2018;22(10):2541-2549.

56. Palomero T, Sulis ML, Cortina M, et al. Mutational loss of PTEN induces resistance to NOTCH1 inhibition in T-cell leukemia. *Nat Med*. 2007;13(10):1203-1210.

57. Allan JN, Furman RR. Current trends in the management of Richter's syndrome. *Int J Hematol Oncol*. 2018;7(4):IJH09.

58. Ding W, LaPlant BR, Call TG, et al. Pembrolizumab in patients with CLL and Richter transformation or with relapsed CLL. *Blood*. 2017;129(26):3419-3427.